Power Ultrasound Assisted Design of Egg Albumin Nanoparticles

Carolina Arzeni, Oscar E. Pérez & Ana M. R. Pilosof

Food Biophysics

ISSN 1557-1858

Food Biophysics
DOI 10.1007/s11483-015-9407-2

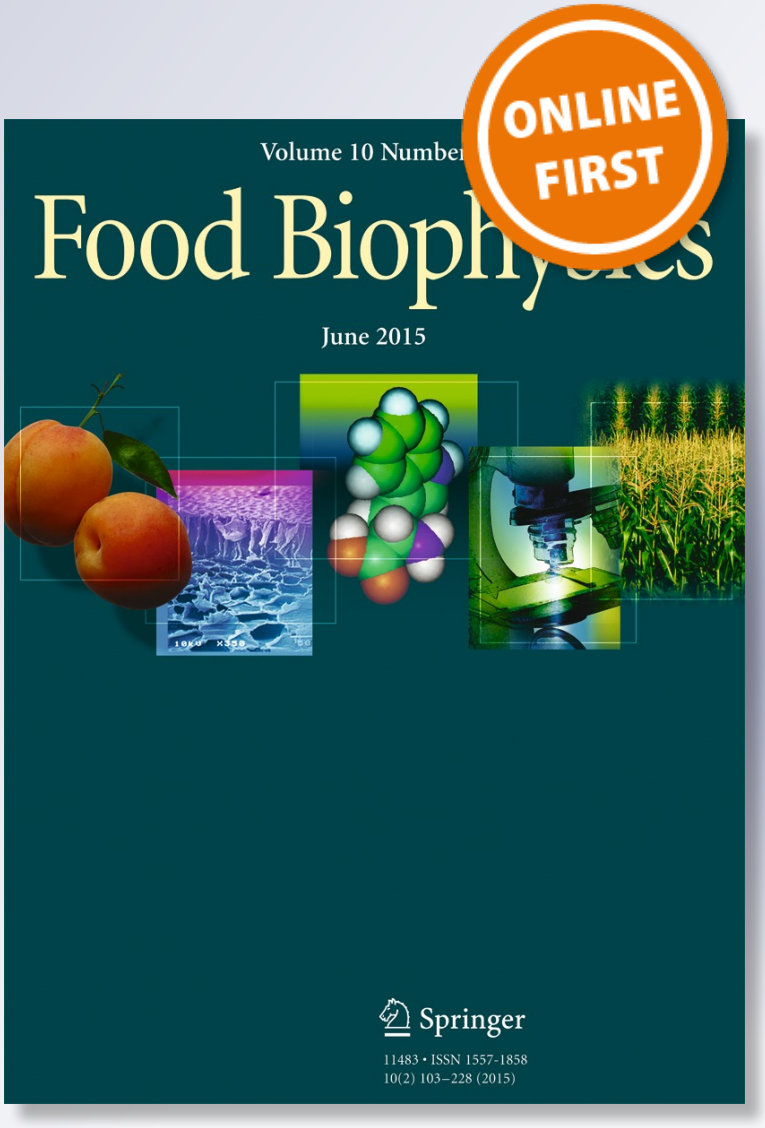

Springer

Food Biophysics
DOI 10.1007/s11483-015-9407-2

ORIGINAL ARTICLE

Power Ultrasound Assisted Design of Egg Albumin Nanoparticles

Carolina Arzeni[1,2] · **Oscar E. Pérez**[1,2] · **Ana M. R. Pilosof**[1,2]

Received: 29 August 2014 / Accepted: 24 June 2015

Abstract The objective of this work was to develop egg white (EW) nanoparticles by application of high intensity ultrasound (HIUS) at different solution pHs and treatment temperatures. At pH 7 HIUS without heating decreased the particle size. In contrast, the use of thermosonication (TS) increased the particle size. At pH 3, the application of both HIUS and TS induced a significant reduction of particle size. at pH 7 zeta potential did not vary significantly when native solutions were sonicated without heating; however a great decrease was observed when TS or heating were applied. At pH 3, sonication decreased the zeta potential of particles but TS or heating increased the charge. By applying TS (85 °C, 20 min and pH 3) a bimodal distribution was obtained, including particles of 295 and 70 nm of diameter. At the same pH, without heating, a monomodal population of 220 nm of diameter was obtained.

Keywords Nanoparticles · Egg white · Ovalbumin · High intensity ultrasound

Introduction

Egg white proteins possess multiple functional properties such as foaming, emulsification, heat setting and binding adhesion. The main EW proteins are ovalbumin, conalbumin and lysozyme [1]. Among so many properties that characterize EW, the ability to aggregate and form gels is one of the most important and the one that makes EW to be extensively used in many food products. Ovalbumin is the major protein in albumen, constituting about 54 % of the total egg white protein [2], and it is the main responsible for the gelling behaviour.

Heated ovalbumin solutions produce transparent, opaque or turbid gels depending on pH, ionic strength and protein concentration. Near the pI (4<pH<6) or at high ionic strength, electrostatic repulsive forces are weak. Thus, the intermolecular attractive forces (usually hydrophobic interactions) induce the formation of random aggregates, resulting in the formation of soft and turbid gels. When the protein molecules bear many charges, i.e., far from the isoelectric point and at low ionic strength, electrostatic repulsive forces hinder the formation of random aggregates, and linear aggregates are formed, resulting in the formation of transparent gels, since the characteristic length scale of the linear particles is smaller than the wavelength of visible light. At intermediate pH and ionic strength, branched flexible aggregates are formed [3]. To this day, there is a large number of research articles referring to pure EW proteins, especially to ovalbumin. However, only a few deal with a commercial EW protein isolate, which is widely used in the food industry.

On the other hand, it is known that HIUS treatment can induce structural modifications of biopolymers. Proteins cleave unpredictably; they are linear polymers but are folded into complex structures involving one or more polymer chains that are often stabilized by covalent, ionic, hydrophobic, and hydrogen bonds. Amino acids with sulfhydryl and phenolic residues can be modified by hydroxyl radicals generated by cavitation bubbles to form new covalent bonds between protein polymer chains. Radicals formed by the cleavage of biopolymers also have the

✉ Ana M. R. Pilosof
apilosof@di.fcen.uba.ar

[1] Departamento de Industrias, Facultad de Ciencias Exactas y Naturales, Universidad de Buenos Aires, Buenos Aires, Argentina

[2] Consejo Nacional de Investigaciones Científicas y Técnicas (CONICET), Buenos Aires, Argentina

Published online: 14 July 2015

potential to recombine into novel polymer structures [4]. The efficiency of HIUS for reducing the particle size of biopolymer solutions has already been proved by many authors [5–17]. Nowadays, the development of biopolymer nanoparticles has a particular importance for the design of food-grade delivery systems to encapsulate, protect and deliver bioactive components. The dimensions of the particles within a delivery system delineate their effects on appearance, rheology, stability, mouthfeel, and release rates [18]. However, limiting size in nanotechnology to the 1–100 nm range excludes numerous material, therefore some expert caution against a rigid definition based on a sub-100 nm size should be considered [19]. Any form of a material that has one or more dimensions in the nanoscale is known as nanomaterial. According to another definition, "nanomaterial" means a natural, or manufactured material containing particles in an unbound state or as an aggregate or as an agglomerate and, where, for 50 % or more of the particles in the number size distribution, one or more dimension is in the range 1–100 nm [20]. Any material that is intentionally produced in the nanoscale to have specific properties or a specific composition is called a manufactured/engineered nanomaterial. Such nanomaterials have different properties when compared with their conventional counterparts [21]. Therefore, it is of interest to study the effect of ultrasound treatment on egg white protein to control the particle size. Then, these nanoparticles could be useful for binding bioactive molecules and act as carriers, for their controlled release at specific sites of the gastrointestinal tract.

In consequence, the objective of this work was to explore the ability of HIUS to design EW nanoparticles by characterizing the particle size distribution and structure of the formed particles.

Materials and Methods

Preparation of Egg White Protein Solutions

EW powder, gently provided by Ovoprot International S.A. (Buenos Aires, Argentina), was used as starting material. The protein content (total basis) of the powder was 88.93±1.18 % (N×6.25) determined by the Kjeldhal method (AOAC, 1980). Solutions at 5 % *w/w* were prepared with double distilled water. Sodium azide (0.02 % *w/w*) was added in order to prevent microbial growth. Solutions were centrifuged for 1 h at 12,857 × *g* and 20 °C (Centrifuge 5804 R, Eppendorf, Hamburg, Germany). The supernatant was used for the determinations. The pH of the supernatant was 7.0±0.1. For the assays made at pH3 the adjustment was made with HCl 1N. All the reactives used here were of analytical grade.

High Intensity Ultrasound Treatment

EW solutions (5 % *w/w*) were sonicated for 5, 10, 15 and 20 min using an ultrasonic processor Vibra Cell Sonics, model VCX 750 (Newtown, Connecticut, USA) with a maximum net power output of 750 W at a frequency of 20 kHz and an amplitude of 20 % (maximum amplitude 40 %, 228 μm). The acoustic power dissipated in the liquid, determined by a calorimetric method according to a previous work [22] was 4.27± 0.71 W. A 13 mm high grade titanium alloy probe threaded to a 3 mm tapered microtip was used to sonicate 5 ml of solution contained in a 15 ml glass tube. Samples were immersed into a glycerine-jacketed bath (Polystat, Cole-Parmer) with water circulating at a constant temperature of 0,5 °C, to dissipate the heat produced during sonication in order to evaluate the effect of HIUS alone, and upon heating at 80 and, 85 °C. Each combination of sonication time and temperature was performed in duplicate.

Particle Size and Zeta Potential Determinations

Particle size of control and sonicated EW solutions was measured by dynamic light scattering (DLS) with a Zetasizer Nano-Zs analyser from Malvern Instruments (Worcestershire, UK). The equipment is provided with a Ne-He laser (633 nm) and a digital correlator, model ZEN3600. The measurements were performed in a fixed angle of 173°, within the range of 0.6 nm to 6 μm, according to the equipment specifications. The samples were diluted at 0.1 % *w/w* in double distilled water and placed into disposable polystyrene cuvettes. Two approaches were utilized to obtain size information. Firstly, Contin's algorithm was used to analyze the data for percentile distribution of particle/aggregate sizes [23]. The size distribution obtained is a plot of the relative intensity of light scattered by particles in various size classes and it is therefore known as an intensity size distribution. If the plot shows a substantial tail, or more than one peak, then Mie theory can be applied to convert the intensity distribution to a volume distribution. This will then give a more realistic view of the importance of the tail or second peak present. However, when transforming an intensity distribution to a volume/mass distribution, there are four assumptions that must be accepted: all particles are spherical; all particles are homogeneous; the optical properties of the particles are known, i.e., the real and imaginary components of the refractive index and; there is no error in the intensity distribution. An understanding of these assumptions is particularly important since the DLS technique itself produces distributions with inherent peak broadening, so there will always be some error in the representation of the intensity distribution. As such, volume and number distributions derived from these intensity distributions are best used for comparative purposes, or for estimating the relative proportions where there are multiple modes, or peaks, and should

never be considered absolute. It is therefore good practice to report the size of the peak based on an intensity analysis and report the relative percentages only (not size) from a volume distribution analysis [24]. Thus, in the present work, the mean particle size of each peak is reported in intensity and the plot of the distribution is reported in volume, in order to visualize the relative contribution of each population. Secondly, a cumulant method was used to find the mean average (Z-av) or the size of a particle that corresponds to the mean of the intensity distribution.

Measurements of zeta potential (ζ) were made with the same analyzer at a fixed angle of 17°. The solutions were diluted at 0.01 % with double distilled water and placed into special folded capillary cells (DTS1060C, Malvern Instruments, Worcestershire, UK). Mean values of two replicates per sample are informed.

Structure Analysis

Confocal Laser Scanning Microscopy

Images of EW nanoparticles suspensions were recorded with a confocal laser scanning microscope (Model FV300, Olympus, UK), provided with an He–Ne laser (543 nm). An objective PLAN APO 60X and a digital zoom of 2.5X were used. Non-covalent labelling of protein was performed with a few drops of 0.02 % *w/w* rhodamine B solution (excitation wavelength 560 nm; emission maximum 625 nm). Digital image files were acquired in multiple.tif format in 1024×1024 pixel resolution.

Atomic Force Microscopy

An aliquot of 5 μl of sample, diluted at $1/10^6$ in double distilled water, was adsorbed to a freshly cleaved mica surface (glued to steel disks), allowed to incubate at ambient temperature, then gently washed with Milli-Q water, and dried under a gentle stream of filtered dry nitrogen. AFM imaging was performed in tapping mode on a Vecco-Digital Instruments microscope, model Multimode (MMAFM) NanoScope IIIa-Quadrex, with a vertical J scanner having a maximal lateral range of approximately 150 μm. Standard silicon cantilevers of 125 μmin length were used for all tapping in air images. The cantilever oscillation frequency was tuned to 280–320 nm, and samples were scanned at 3–5 lines/s. Images were processed with NanoScope software [25] by applying flattening to remove background slope. The dimensions of the nanoparticles structures have been quantified, using section analysis, in terms of the vertical height and horizontal diameter. The vertical height corresponds to the maximum vertical distance measured from the top of the protein surface to the neighboring mica. The horizontal diameter corresponds to the measured diameter of the protein structure at half the vertical height. This measurement has been used to describe the lateral dimension of the protein structure, rather than the horizontal diameter at zero vertical height, to minimize the influence of tip induced broadening [26, 27].

Results and Discussion

Particle Size Distribution of EW at pH 3 and 7

The initial particle size distribution of EW solutions, determined at 0.1 % *w/w* by dynamic light scattering (DLS) is shown in Figs. 1 and 3. At pH 7, the particle size distribution of EW solution exhibited a main wide peak with a size of 220 nm in intensity, including particles from 51 to 1281 nm. A smaller population of about 5560 nm was also apparent near the limit of detection of the equipment. Mine [28] obtained for an ovalbumin solution heated at 80 °C for 20 min a size distribution that included a peak below 10 nm that was ascribed to free ovalbumin, and two peaks of higher sizes, comparable to the ones obtained in this work, which corresponded to aggregates formed by the heat treatment. In the present work, these aggregates could have been generated during the spray drying process applied by the manufacturer for EW dehydration. On the other hand, at pH 3, the particle size distribution of EW solution showed a main peak at 1106 nm in intensity, ranging from 106 to 3091 nm, higher than that present at pH 7. Another population of about 5560 nm was also seen near the upper limit of detection of the equipment.

Influence of HIUS without Heating on EW Particle Size Distribution

At pH 7, the application of HIUS reduced the particle size, as shown by the decrease of the intensity of the main peak and the simultaneous increase of the population of particles below 100 nm (Fig. 1a). The peak observed at 5560 nm was also reduced by HIUS treatment.

As stated before, the particle size distribution of the native EW solution at pH 3 included bigger particles than at pH 7. At pH 3, the application of HIUS caused a strong reduction of the particle size after 5 min of processing, which continued to decrease with time, though at a lower rate (Fig. 1b). The size distribution was monomodal, ranging from 79 to 615 nm with a maximum at 220 nm, for the longest processing time of 20 min. Likewise, Gordon et al. [6] found that the particle size of WPI solutions at 7.5 % *w/w* decreased under the effects of ultrasounds at room temperature and this reduction was greater during the first 2 min of sonication, and then leveled off after 5 min of processing. In this regard, Iida, Tuziuti, Yasui, Towata and Kozuka [10] found that depolymerization of starches of different sources using ultrasound was intense

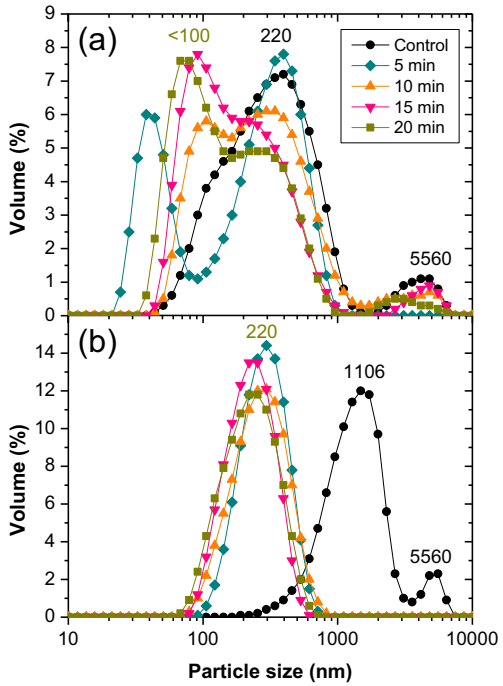

Fig. 1 Particle size distribution of EW solutions at pH 7 (**a**) and 3 (**b**), sonicated at 5 % *w/w* for 0–20 min without heating

during the initial period of 10–30 min and thereafter it proceeded slowly.

It may be concluded that HIUS treatment of EW at pH 7 generated particles with lower size than the ones produced at pH 3. However, at pH 3 a monomodal distribution of 220 nm could be obtained.

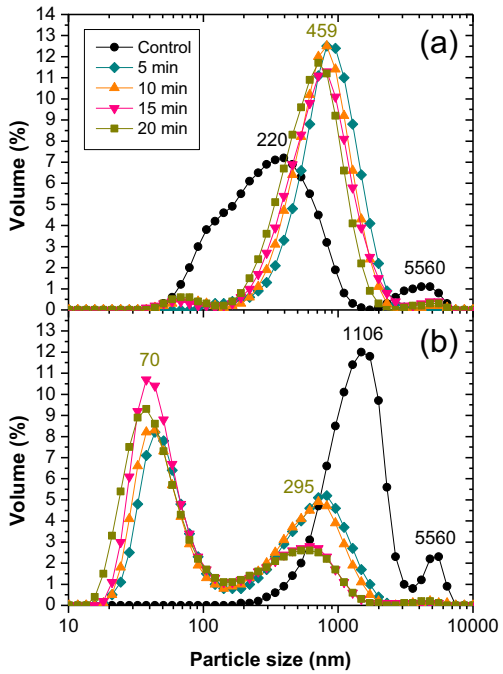

Fig. 3 Particle size distribution of EW solutions at pH 7 (**a**) and 3 (**b**), thermosonicated at 5 % *w/w* for 0–20 min at 85 °C

Influence of HIUS upon Heating (Thermosonication) on EW Particle Size Distribution

First of all, the effect of heating time at 80 or 85 °C on the particles size was studied. Similar trends were observed at 80 or 85 °C at both pHs; particle size increased continuously over the heating time as a result of denaturation and aggregation of proteins. The only difference was that the rate of aggregation at 85 °C was higher than at 80 °C. At pH 3, the degree of protein aggregation was higher than at pH 7, for both temperatures, which caused the particles to sediment in the cuvette during DLS measurement. Thus, only samples heated at pH 7 could be measured by this technique (Fig. 2), except for the sample heated at 85 °C for 20 min that could not be measured for the same reason as explained before. Hagolle, Launay and Relkin [29] found by PAGE-electrophoresis that heating 5 % *w/w* solutions of ovalbumin at pH 3 produced a higher percentage of aggregates at lower temperatures than at pH 7. They also reported that non-covalently bound aggregates were formed at pH 3 beyond 52 °C, followed by the creation of intermolecular β-sheet structures, while at pH 7 covalently bound aggregates were developed.

The solutions heated at neutral pH were opaque, while at acid pH were transparent. Similarly, Qin [30] obtained transparent, turbid and opaque gels after heating fresh EW at 80 °C for 1 h at pH 3.5, 5.5 and 7.5, respectively. When applying the TS treatment at 80 or 85 °C, similar trends were observed for both heating conditions. Thus, only the results at 85 °C are shown. At pH 7, the particle size increased after 5 min of TS; the main peak diameter changed from 220 to 664 nm in intensity (Fig. 3a). Then, the magnitude of the increase was lower at higher times (615, 531 and 459 nm after 10, 15 and 20 min of processing, respectively). These results show that the aggregation produced by the thermal treatment would prevail over the disruption caused by HIUS application, although sonication would not allow particles to grow continuously as during the thermal treatment. Similarly, Gordon & Pilosof [6] found that heating WPI solutions (12 % *w/w*, neutral pH) at 85–93 °C with simultaneous sonication for 10 min strongly

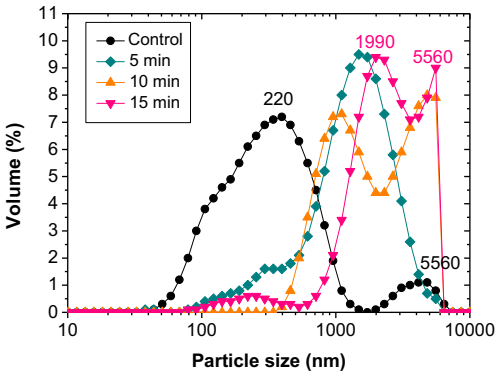

Fig. 2 Particle size distribution of EW solutions (5 % *w/w*) at pH 7 heated for 0–20 min at 85 °C

increased the particle size in comparison with the untreated sample.

Contrarily, when EW was thermosonicated at pH 3 a strong decrease of the particle size was observed (Fig. 3b). However, the size distribution was bimodal, with most of the particles having 70 nm of diameter. The other minor population was at 459 nm, after 5 min of processing and then gradually decreased to 396, 319 and 295 nm after 10, 15 and 20 min, respectively. Thus, at pH 3 the disruption effect caused by HIUS prevailed over the aggregation effect induced by heating, resulting in a net decrease of particle size. The difference found at pH 3 in comparison to pH 7 may be related to the higher initial particle size and also the higher increase in size observed after heating EW solutions at pH 3, because the chances of being attacked by the cavitation energy increase with the size of particles, since smaller particles have shorter relaxation times and, thus, can alleviate the sonication stress easier [31].

Evolution of Average Size of EW Particles

In order to have a global view of the changes in size caused by the applied treatments, the average particle size (Z-av) of EW at both pHs is depicted in Fig. 4. At pH 7, HIUS treatment produced a slight decrease in Z-av, while at pH 3, it induced a remarkable reduction of Z-av, probably because the size of the starting particles were bigger than at pH 7 and could be more easily disrupted by sonication. Heating caused a continuous increase in Z-av along time. As stated before, samples heated at pH 3 could not be measured by this technique; therefore, only the samples at pH 7 are shown (Fig. 4a). The application of TS at pH 7 produced a rise in the average size, with a maximum at the first 5 min of treatment. This could be because at the beginning, the particles might be too small to be attacked by ultrasound waves, so they only aggregate by the effect of heat. But this phenomenon continues up to a critical size at which ultrasound starts to disrupt the particles, controlling the increase of particle size along the rest of the processing time. On the other hand, at pH 3 TS resulted in a reduction of Z-av, higher than the one observed by HIUS application without heating, and can be attributed to the fact that the effects of ultrasound are more evident on the more aggregated structures. The overall outcome of the TS treatment at pH 7 was opposite to the one obtained at pH 3, maybe because the covalently bound aggregates that have been already proved to develop at pH 7 are not as easy to disrupt as the non-covalently bound aggregates formed at pH 3.

Evolution of Surface Charge of EW Particles

Figure 5 shows the evolution of particles surface charge upon treatment time. The particles of native EW at pH 7 and pH 3

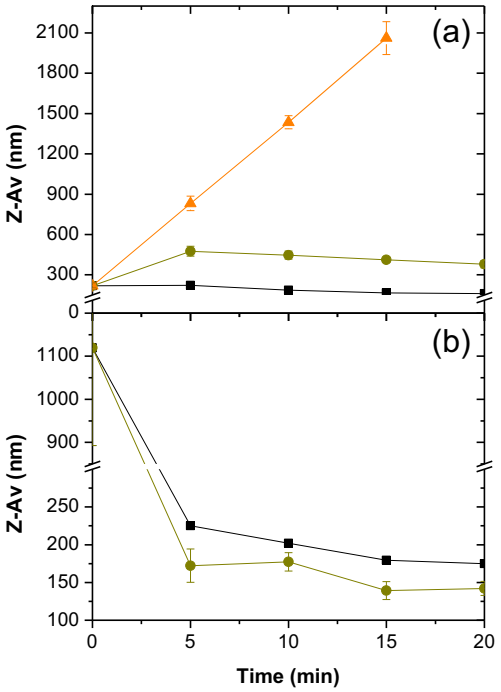

Fig. 4 Evolution of Z-av of EW solutions, 5 % *w/w*, at pH 7 (**a**) and pH 3 (**b**), sonicated (■), heated at 85 °C (▲) and thermosonicated at 85 °C (●) for 0–20 min

had a ζ potential of -15.9±1.1 and +22.7±0.5, respectively. These were comparable to previously reported values for a set of commercial samples of spray-dried EW (dispersed at 1 % in 0.01 M phosphate buffer), which ranged from -16.4 to -29.5, at pH 7, and from +12.6 to +20.9, at pH 3 [32]. At pH 7, there

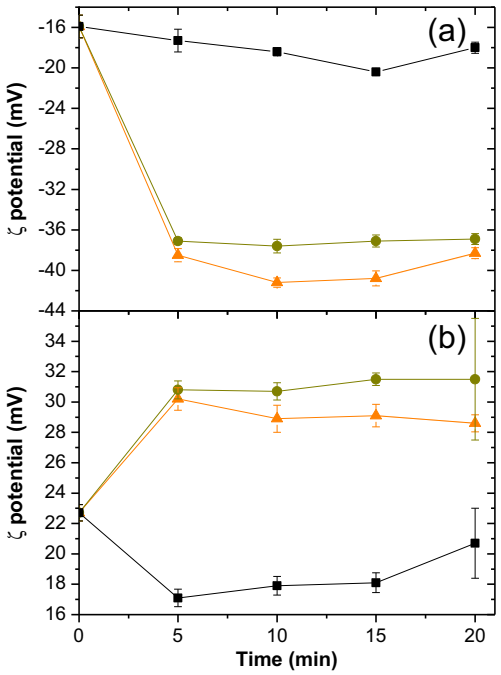

Fig. 5 Evolution of ζ potential of EW solutions, 5 % *w/w*, at pH 7 (**a**) and pH 3 (**b**), sonicated (■), heated at 85 °C (▲) and thermosonicated at 85 °C (●) for 0–20 min

was no significant change of ζ potential when EW was sonicated without heating; however, a dramatic increase in ζ potential (~ −40 mV) was observed when heating EW at 80 or 85 °C (Fig. 5a), suggesting that the exposure of charges to the surface of the particle would be enhanced by protein denaturation and aggregation [33]. For the TS treatment, the thermal effect seemed to determine the ζ potential of the particles, as it was similar to the obtained for heated EW particles. At pH 3, EW particles had a positive global surface charge which was then decreased by sonication. By only heating EW, an increase in charge was observed (~ +30 mV), not as large as at pH 7. The TS also increased the charge (Fig. 5b). As for pH 7, denaturation and aggregation induced by heating exposed more charged groups to the surface of EW particles than sonication. Zeta potential is an important and useful indicator to predict and control the stability of colloidal suspensions. The greater the zeta potential, the more likely the suspension will be stable because charged particles repel one another and thus overcome the natural tendency to aggregate [34]. As a limit between stable and unstable suspensions, ζ=±30 mV may be assumed [35]. However, zeta potential should not be used as a stand-alone predictive tool for the evaluation and optimization of colloidal stability, since other physical forces may be involved in this phenomenon [36].

Structure of EW Nanoparticles

Two kinds of EW nanoparticles were selected based on the particle size distributions: those obtained by HIUS and those by TS at 85 °C, for 20 min, at pH 3 (referred to as USN and TSN, respectively, from now on). The first EW nanoparticles (USN) were chosen since they presented a monomodal distribution of 220 nm of diameter (Fig. 2b). TSN were chosen because they were constituted mostly by a population of small particle size (~70 nm), though the distribution also included particles of 295 nm (Fig. 3b). Confocal laser scanning microscopy was first used for their characterization. The images of both types of EW nanoparticles manifested a homogeneous microstructure with subtle differences (Fig. 6). TSN showed fewer void spaces and the particles density seemed to be higher. So, with the purpose of getting an insight on the possible differentiation between the nanoparticles, further analysis within the nano scale was performed by atomic force microscopy (AFM). USN were found to be rounded and regular and had approximately 14 nm of diameter (Fig. 7a). At first sight, this value was not comparable with the hydrodynamic diameter obtained by DLS for this system (220 nm). It is noteworthy that in the AFM technique applied here the samples were measured in air, after washing and drying them. Therefore, not all the particles present in the solution may remain adsorbed on the mica surface as, upon washing, a large fraction of protein is removed from the surface [37]. Besides, it is known that in DLS small particles may be underestimated, as large particles scatter much more light than small ones. So, USN samples were filtered by 0.22 and 0.02 μm in order to check the presence of particles smaller than 220 nm (Fig. 8). When the sample was filtered by 0.22, μm a population of 24 nm and another one of 6.5 nm were detected by DLS. The first one was attributed to protein aggregates [29] and the other one, to free ovalbumin, the main EW protein, according to the estimation of the hydrodynamic diameter made by the software using the known molecular weight of this protein, which is 45 kDa. Other EW proteins might be included within the range of the same peak (3.6–16 nm), e.g., conalbumin, ovomucoid, and lysozyme, among others. When the sample was further filtered by a 0.02 μm pore, only the peak of 6.5 nm was observed. Still after filtering the sample, AFM and DLS diameters did not match. However, the particles seen by AFM had a very high diameter/height ratio, therefore, it was probable that during the drying step of the sample preparation the particles crush over the mica surface, acquiring a disc shape and, in consequence, a larger diameter. So, these disc-shaped particles could be the ones of 6.5 nm measured by DLS. To confirm this, the particle volume was calculated according to Chávez Benavides [38], based on the data obtained by each technique. It is worth to clarify that these calculations are estimative and for the purpose of qualitatively identify the corresponding population only. As in DLS the diameter is obtained assuming spherical particles, the volume was calculated as: $V_{DLS}=4/3\times(\pi r^3)$, with r being the hydrodynamic radius. The volume of the disc-shaped particles observed by AFM was approximated to a flat cylinder and was calculated as: $V_{AFM}=(\pi r^2)\times h$, being r and h the radius and the height obtained from the particle profile analysis, by AFM. The calculated volumes were 144 and 120 nm^3, for DLS and AFM, respectively. AFM gives the physical diameter of the particles on a substrate, while DLS provides a hydrodynamic diameter, which takes into account the hydration sphere that surrounds the particle. Therefore, the differences in the calculated volumes are expected. Besides, aggregates seen by DLS might not be retained on the mica surface and the population observed by AFM could correspond mainly to ovalbumin.

On the other hand, TSN were more heterogeneous (Fig. 7b), having two kinds of particles: one class composed of linear strings of different lengths and another one that had circular shape, with irregular borders, of about 10–30 nm of diameter. At pH 3, EW proteins aggregate by heat forming linear polymers also known as “strings of beads” and the

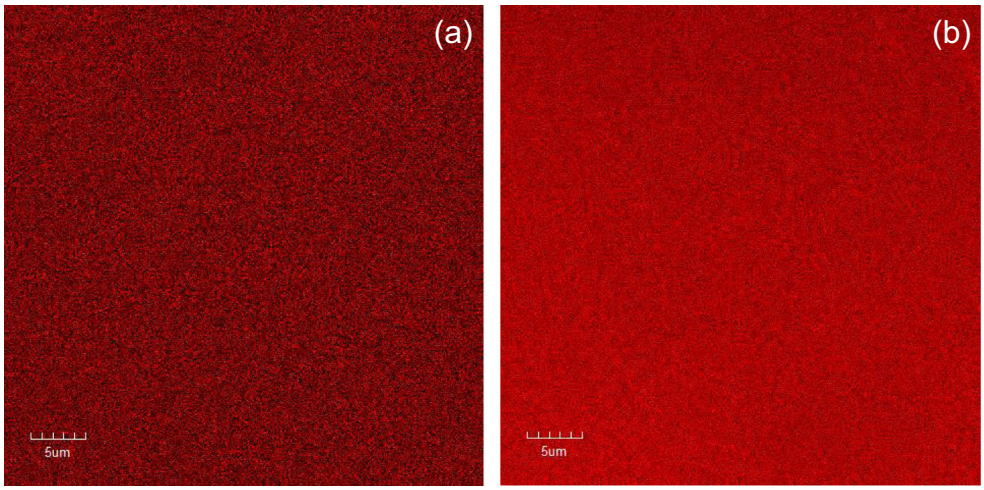

Fig. 6 Confocal laser scanning microscopy images of (**a**) USN and (**b**) TSN at 5 % *w/w*

application of TS causes the rupture of these strings in smaller fragments. According to DLS size distribution, two main populations were found: one of large particles (295 nm), which may correspond to linear aggregates, and another one of smaller size (70 nm), that may contain the particles of 10–30 nm and also small fragments of linear aggregates.

In conclusion, neither DLS nor AFM could be used separately to characterize the nanoparticles size. On the one hand, AFM technique could be used to investigate the "tail" of the particle distribution, while DLS is significantly less sensitive for small particles present in a wider size distribution [39], although it provides an easy, fast and reliable measurement for monodisperse samples. On the other hand, AFM scans cannot always be used to accurately calculate the ratio of nanoparticle sizes used in the nanoparticle mixtures, as deposition methods may skew the size distribution [40].

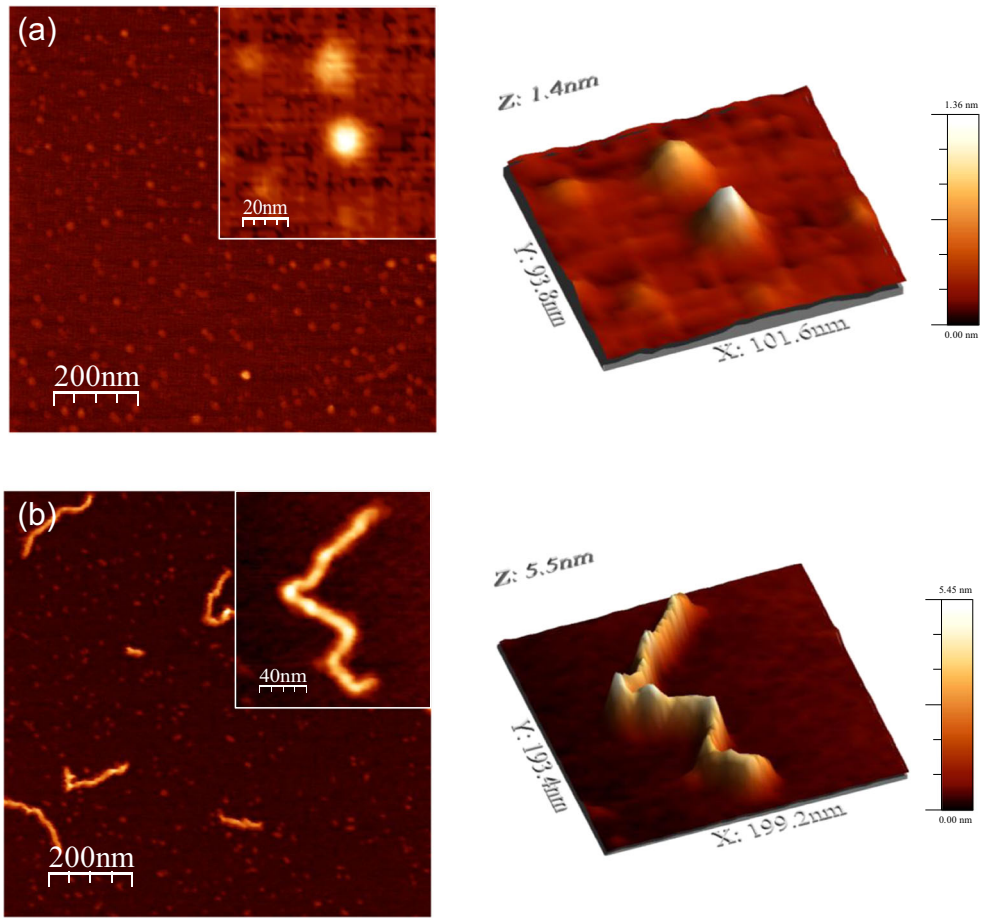

Fig. 7 Atomic force microscopy images (top and 3D views) of (**a**) USN and (**b**) TSN. The scale at the right corresponds to the maximum peak to valley distance

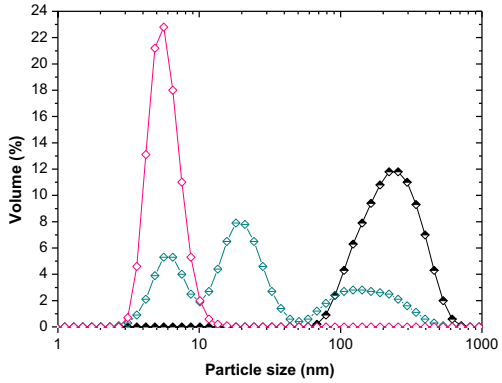

Fig. 8 Particle size distribution of USN at pH 3, unfiltered (◆), filtered by 0.22 μm (◇) and by 0.02 μm (◇)

Conclusion

Power ultrasound proved to be a potential green technology to design EW nanoparticles. By controlling the conditions of the sonication treatment, i.e., temperature and time, as well as pH conditions, it was possible to control the particle size of EW in the range of 70 to 459 nm.

The major modifications occurred during the first minutes of sonication, and no significant changes were observed at longer processing times.

These particles could be used in different applications with specific particle size requirements, such as developing new textures and sensations, controlling the release of flavours, increasing the bioavailability of nutritional components, among others. In particular, the nanoparticles designed in this work at pH 3 could have a promising performance for the binding and delivery of labile bioactive compounds, a topic that will be addressed in our next contribution.

Acknowledgments This work has been done with the support of the University of Buenos Aires (Grant: 20020120200087BA), the Consejo Nacional de Investigaciones Científicas y Técnicas (Grant: 11220110100317) and the Agencia Nacional de Promoción Científica y Tecnológica (Grant: PICT 2011–1279).

References

1. Y. Mine, Trends Food Sci. Technol. **6**(7), 225–232 (1995)
2. E. Li-Chan, W. D. Powrie and S. Nakai, in *Egg science and Technology*, ed. by W.J. Stadelman, O.J. Cotterill (Food Products Press, New York, 1995), pp. 105–175
3. M. Weijers, L.M.C. Sagis, C. Veerman, B. Sperber, E. van der Linden, Food Hydrocoll. **16**(3), 269–276 (2002)
4. K. Vilkhu, R. Manasseh, R. Mawson, M. Ashokkumar, in *Ultrasound technologies for food and bioprocessing*, ed. by H. Feng, G.V. Barbosa-Cánovas, J. Weiss (Springer Science+ Business Media, New York, 2011), p. 364
5. N. Kardos, J.-L. Luche, Carbohydr. Res. **332**(2), 115–131 (2001)
6. L. Gordon, A. Pilosof, Food Biophys. **5**(3), 203–210 (2010)
7. A.R. Jambrak, V. Lelas, T.J. Mason, G. Krešić, M. Badanjak, J. Food Eng. **93**(4), 386–393 (2009)
8. M. Villamiel, P. de Jong, J. Agric, Food Chem. **48**(2), 472–478 (2000)
9. C.-H. Tang, X.-Y. Wang, X.-Q. Yang, L. Li, J. Food Eng. **92**(4), 432–437 (2009)
10. Y. Iida, T. Tuziuti, K. Yasui, A. Towata, T. Kozuka, Innov. Food Sci. Emerg. Technol. **9**(2), 140–146 (2008)
11. J.P. Lorimer, T.J. Mason, T.C. Cuthbert, E.A. Brookfield, Ultrason. Sonochem. **2**(1), S55–S57 (1995)
12. R.H. Chen, J.R. Chang, J.S. Shyur, Carbohydr. Res. **299**(4), 287–294 (1997)
13. A.R. Jambrak, T.J. Mason, V. Lelas, G. Kresic, LWT Food Sci. Technol. **43**(2), 254–262 (2010)
14. T. Furukawa, S. Ohta, Agric. Biol. Chem. **47**(4), 745–750 (1983)
15. S. Baxter, S. Zivanovic, J. Weiss, Food Hydrocoll. **19**(5), 821–830 (2005)
16. B. Zisu, R. Bhaskaracharya, S. Kentish, M. Ashokkumar, Ultrason. Sonochem. **17**(6), 1075–1081 (2010)
17. M. Ashokkumar, J. Lee, B. Zisu, R. Bhaskarcharya, M. Palmer, S. Kentish, J. Dairy Sci. **92**(11), 5353–5356 (2009)
18. D.J. McClements, *Food Emulsions: principles, practice and techniques* (CRC Press, Boca Raton, 2005)
19. National Science and Technology Council, (United States, 2014)
20. The European Commission, (Official Journal of the European Union, Brussels, 2011)
21. B.S. Sekhon, Nanotechnol. Sci. Appl. **7**, 31–53 (2014)
22. C. Arzeni, K. Martínez, P. Zema, A. Arias, O.E. Pérez, A.M.R. Pilosof, J. Food Eng. **108**(3), 463–472 (2012)
23. P. Štěpánek, *Dynamic Light Scattering. The Method and Some Applications*, (1993), pp. 177–241
24. Dynamic light scattering - common terms defined (2014)
25. I. Horcas, R. Fernández, J. M. Gómez-Rodríguez, J. Colchero, J. Gómez-Herrero, A. M. Baro, Rev. Sci. Instrum. **78**(1) (2007)
26. J.S. Villarrubia, J Res Natl. Inst. Stand. Technol. **102**(4), 425–454 (1997)
27. L.V. Najbar, R.F. Considine, C.J. Drummond, Langmuir **19**(7), 2880–2887 (2003)
28. Y. Mine, J. Agric, Food Chem. **44**(8), 2086–2090 (1996)
29. N. Hagolle, B. Launay, P. Relkin, Colloids Surf. B: Biointerfaces **10**(4), 191–198 (1998)
30. L. Qin, (University of British Columbia 1997)
31. M.L. Tsaih, R.H. Chen, J. Appl. Polym. Sci. **90**(13), 3526–3531 (2003)
32. E. S. Y. Cheng, (University of British Columbia 2001)
33. N. Hagolle, P. Relkin, D.G. Dalgleish, B. Launay, Food Hydrocoll. **11**(3), 311–317 (1997)
34. E.I. Benitez, J.E. Lozano, Lat. Am. Appl. Res. **36**, 163–168 (2006)
35. P. Sherman, in *Industrial Rheology* (Academic Press Inc., 1970), pp. 97–183
36. M. Wagner, K. Reiche, A. Blume, P. Garidel, Colloids Surf. Physicochem. Eng. Asp. **415**, 421–430 (2012)
37. O. Younes-Metzler, R.N. Ben, J.B. Giorgi, Colloids Surf. B: Biointerfaces **82**(1), 134–140 (2011)
38. J. L. Chávez Benavides, Tesis Doctoral (University of Florida, 2008)
39. D. Chicea, E. Indrea, C.M. Cretu, J. Optoelectron. Adv. Mater. **14**(5–6), 460–466 (2012)
40. C. Hoo, N. Starostin, P. West, M. Mecartney, J. Nanopart, Res. **10**(1), 89–96 (2008)